

# Exploring the Energy Profile of the $Q_A^-$ to $Q_B$ Electron Transfer Reaction in Bacterial Photosynthetic Reaction Centers: pH Dependence of the Conformational Gating Step<sup>†</sup>

Qiang Xu and M. R. Gunner\*

Department of Physics, Room J419, City College of New York, 138th Street and Convent Avenue, New York, New York 10031

Received September 24, 2001; Revised Manuscript Received December 27, 2001

**ABSTRACT:** Both large- and small-scale conformational changes are needed as proteins carry out reactions. However, little is known about the identity, energy of, and barriers between functional substates on protein reaction coordinates. In isolated bacterial photosynthetic reaction centers, the electron transfer from the reduced primary quinone,  $Q_A^-$ , to the secondary quinone,  $Q_B$ , is rate limited by conformational changes at low pH and by proton binding at high pH. The kinetics and thermodynamics of this reaction were determined between 200 and 300 K from pH 6 to pH 10.5. A model with two substates of the reactant,  $P^+Q_A^-Q_B$ , one protonated (state A) and one unprotonated ( $\alpha$ ), and one state of the product,  $P^+Q_AQ_B^-$  (B), was able to simulate the dependence of the rate on temperature and pH fairly well. The equilibrium between the three states were measured in situ at each temperature. Proton binding ( $\alpha$  to A transition) has a favorable  $\Delta H$  and unfavorable  $\Delta S$  as does the conformational changes required for electron transfer at low pH (A to B). The pK for the A to  $\alpha$  transition is 9.7 at room temperature, consistent with previous measurements, and  $\approx 13.5$  at 200 K. The activation barriers were determined for each transition. Both the  $\alpha$  to A and the A to B transitions are limited primarily by the activation enthalpy with modest  $\Delta S^\ddagger$ .

Reaction rates in proteins are often determined by how fast the reactant can undergo conformational changes (1, 2). Energy barriers associated with required transformations cause reactions to slow and then stop at low temperature (3–6). Large-scale conformational changes have been seen in time-resolved structural studies (7, 8) and by trapping reaction intermediates (9–11). Crystallographic evidence for substrate and product being bound in different positions has been found in photosynthetic reaction centers (RCs)<sup>1</sup> trapped in different redox states (12). However, if small-scale motions such as changes in protonation state or hydrogen bonding are required, these will not be seen in any but the very highest resolution protein structures.

Various techniques are becoming available to monitor the states along reaction paths. Rapid initiation of single turnover reactions by laser-induced temperature jumps has revealed multiple substates for substrate binding to lactate dehydrogenase (13). The temperature dependence of NMR structure

factors has followed changes in calmodulin entropy (14). Analysis of NMR relaxation parameters identified changes in structure and mobility in active and inactive signaling protein (15). Bacterial photosynthetic reaction centers (RCs) also provide an excellent model system for the detailed study of reaction substates and the barriers between them (16, 17). It is possible to initiate reactions in RCs with a pulse of light, allowing synchronized, single turnover measurements over a wide range of time scales. Reactions are reversible, allowing signal averaging. The protein is functional, and reaction rates can be determined even at cryogenic temperatures, providing a large scope for thermodynamic measurement. Last, it is possible to determine reaction free energies, and associated  $\Delta H$ , and  $\Delta S$  at temperatures as low as 250 K for several intraprotein reactions (16).

RCs are the membrane proteins that facilitate the conversion of light to chemical energy in purple non-sulfur photosynthetic bacteria. On absorption of a photon, a series of electron transfers between cofactors bound to the protein yield a transmembrane separation of charge (Figure 1) (18). The electron transfer from the reduced primary quinone,  $Q_A^-$ , to the secondary quinone,  $Q_B$ , is rate limited by conformational changes in isolated RCs with the native ubiquinone as  $Q_A$  and  $Q_B$  (19). However, RCs can be trapped in an active conformation where the electron transfer itself is now rate limiting. These conditions are met in the native chromatophore membranes (20) and in hybrid RCs with the ubiquinone  $Q_A$  replaced by a lower potential quinone (21, 22). In addition, when RCs are frozen in the product  $P^+Q_B^-$  state, they return to the ground state in a new conformation. Now electron transfer occurs with high yield at low temperature

<sup>†</sup> We are grateful for the financial support from the Department of Agriculture (CREES 2001-35318-11190) and from the NIH (RR03060) for maintenance of central facilities.

\* To whom correspondence should be addressed. Telephone: 212-650-5557. Fax: 212-650-6940. E-mail: gunner@sci.cuny.cuny.edu.

<sup>1</sup> Abbreviations: RC(s), reaction center(s); P, bacteriochlorophyll dimer which is the primary electron donor;  $Q_A$  and  $Q_B$ , primary and secondary quinone electron acceptors;  $P^+Q_A^-$  and  $P^+Q_B^-$ , reactant ( $P^+Q_A^-Q_B$ ) and product ( $P^+Q_AQ_B^-$ ) redox states; A and  $\alpha$  substates, protonated and unprotonated forms of  $P^+Q_A^-$ ; A\*, substate of  $P^+Q_A^-$  with a low barrier for electron transfer to  $Q_B$ ; B and  $\beta$ , protonated and unprotonated  $P^+Q_B^-$  substates.  $K_{(A)B}$  and  $k_{(A)B}$ , effective equilibrium and rate constants between all subpopulations of  $P^+Q_A^-$  ( $\alpha$ , A, and A\*) and all substates of  $P^+Q_B^-$  under the conditions of measurement. All equilibrium and rate constants have a two-letter subscript. The first letter refers to the reactant and the second to the product substate.

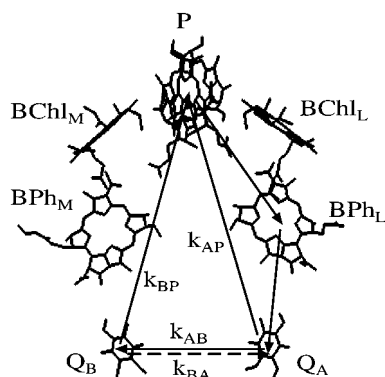


FIGURE 1: Cofactor arrangement and electron transfer pathway in *Rb. sphaeroides* RCs.  $Q_A$  is reduced in  $\approx 150$  ps via  $BPh_L$ , leaving an oxidized  $P^+$ . Then, either  $Q_B$  is reduced at  $k_{(A)B}$  or electron transfer to  $P^+$  at  $k_{(A)P}$  ( $10$  s $^{-1}$ ) re-forms the ground state.  $k_{(A)B}$  and  $k_{(A)P}$  are the effective rate constants for electron transfer from the appropriate distribution of  $P^+Q_A^-$  substates ( $\alpha$ , A, and A\*) under the conditions of measurement. The quantum efficiency  $\Phi$  is decided by the competition between these two processes (eq 1). The substates of  $P^+Q_A^-Q_B$  and  $P^+Q_A^-Q_B^-$  remain at equilibrium. Electron tunneling from either reduced quinone to  $P^+$  returns the system to the ground state. However,  $k_{(A)P}$  is 100 times faster than  $k_{BP}$  ( $0.1$  s $^{-1}$ ) (see eq 3).

without the need to cross the barrier imposed by the normal conformational changes (17, 23).

X-ray crystallography (12, 24) and other experimental (17, 25–28) and computational (29–34) techniques have been used to characterize the conformational change in RCs. In the crystal structure of RCs frozen under illumination in an active state,  $Q_B$  is about  $2.7$  Å closer to  $Q_A$  than in protein frozen in the dark. The shift of the quinone position has been proposed to be the conformational gating step (12, 24). Other studies suggest that shifts of internal protons or changes in hydrogen-bonding pattern may also play a role (17, 30, 32).

RCs can be prepared so the electron transfer from  $Q_A^-$  to  $Q_B$  is gated by a conformation change with a substantial barrier or where the reaction is rapid with little activation energy. To better characterize different reactant substates, the reaction was investigated as a function of temperature and pH. The free energy of the electron transfer from  $Q_A^-$  to  $Q_B$  was determined from room temperature to 260 K from pH 6 to pH 10.5. Some conformational change determines the rate at low pH, while at high pH proton binding becomes rate limiting. The activation enthalpy and entropy for each barrier was found.

## MATERIALS AND METHODS

Isolation of *Rhodobacter sphaeroides* engineered poly-histidine-tagged RCs (35) and ubiquinone reconstitution of  $Q_B$  have been described previously (17). pH buffers (10 mM), Mes (pH 5.5–6.5), Hepes, (6.9–8.0), Tris, (7.5–8.5), Ches (8.6–10.0), and Caps (9.7–11.1) were used (ranges in parentheses for pHs at 25 °C). At 5 °C the pH is 0.5–0.6 unit higher for all buffers except Mes and Hepes where the pH increases by 0.2–0.3 unit. This is consistent with previous reports (36–39). The effect of the temperature dependence of the pH on the derived values will be explored below.

The low-temperature optical setup has been described in detail previously (17). The charge recombination kinetics were measured by monitoring the decay of the  $P^+$  signal at

430 nm with a photomultiplier (Thorn EMI 9798QB). A  $10$  μs xenon flash lamp with a long-wavelength pass filter (750 nm) provided the actinic light. The RC concentration was 3–4 μM. The sample was cooled in an APD (CSW202A) closed-cycle helium cryostat. The measurement started 15 min after the set temperature was reached. The results from 10 flashes at 2 min intervals were averaged. The optical transients were fitted to a two-exponential function using the nonlinear least-squares fitting algorithm in the program IGOR Pro (WaveMetrics). The kinetic model was simulated with Mathematica 3.0 (Wolfram Research).

## RESULTS

The rate of electron transfer from  $Q_A^-$  to  $Q_B$  ( $k_{(A)B}$ ) was obtained from the quantum yield ( $\Phi$ ) for forming the  $P^+Q_B^-$  redox state ( $k_{(A)B}$  is the rate given the distribution of  $P^+Q_A^-$  substates under conditions of measurement). When  $P^+Q_A^-$  is formed by the actinic flash, the electron on  $Q_A^-$  can go either forward to reduce  $Q_B$  (at  $k_{(A)B}$ ) or back to  $P^+$  (at  $k_{(A)P}$ ), re-forming the ground state (Figure 1). Since the reactant  $P^+Q_A^-$  decays at  $k_{(A)B} + k_{(A)P}$ ,  $k_{(A)B}$  cannot be measured when it is much slower than  $k_{(A)P}$ ;  $k_{(A)B}$  is determined most accurately from  $\Phi$  when  $k_{(A)B} \approx k_{(A)P}$  (40); and it can be measured directly when  $k_{(A)B} \gg k_{(A)P}$ . Thus,  $\Phi$  provides a limited window on  $k_{(A)B}$ . The direct measurement of the submillisecond  $k_{(A)B}$  is difficult since there are only small differences in the RC spectra to differentiate RCs with  $Q_A^-$  or  $Q_B^-$  (17, 21, 41). In contrast, measurement of  $\Phi$  used here follows the large changes in absorption as  $P^+$  returns to P on the millisecond time scale.

$\Phi$  is determined given the amplitude of the slow ( $A_S$ ) and fast ( $A_F$ ) components of the  $P^+$  charge recombination. The slower component ( $<1$  s $^{-1}$ ) follows charge recombination from  $P^+Q_B^-$  while the faster component ( $\sim 10$  s $^{-1}$ ) is the charge recombination from  $P^+Q_A^-$  (17). Thus

$$\Phi = \frac{A_S}{A_S + A_F} = \frac{k_{(A)B}}{k_{(A)B} + k_{(A)P}} \quad (1)$$

Given  $k_{(A)P}$ ,  $\Phi$  provides  $k_{(A)B}$ .  $k_{(A)P}$  can be measured independently in RCs with no  $Q_B$  and is essentially temperature (42, 43) and pH (44) independent. In the samples used here the RCs are 80–95% saturated with ubiquinone  $Q_B$ . The fraction which cannot form  $P^+Q_B^-$  is determined at room temperature. Here  $\Phi$  is  $\approx 1$  if the  $Q_B$  site is occupied, since  $k_{(A)B} \gg k_{(A)P}$ . The appropriate amplitude is subtracted from  $A_F$  before  $\Phi$  is calculated, which assumes  $Q_B$  site occupancy is temperature independent. Equation 1 assumes single rate constants for  $k_{(A)B}$  and  $k_{(A)P}$ . The impact of a distribution of rates on the analysis will be discussed below.

The temperature dependence of  $Q_B^-$  formation was measured from pH 6 to pH 10.5 in the temperature range 180–300 K (Figure 2).  $\Phi$  decreases as the temperature is lowered until no  $Q_B^-$  is formed. At higher pH the reaction freezes out at warmer temperature. At pH near 9.7, the temperature dependence of  $\Phi$  has a more stretched, bimodal shape. The temperature-dependent decrease in  $\Phi$  monitors the slowing of the  $Q_A^-$  to  $Q_B$  electron transfer rate  $k_{(A)B}$ . The pH dependence of  $\Phi$  indicates that the reaction is dependent on proton binding.

*Model of the Reaction.* To fit the temperature and pH dependence of  $\Phi$  (Figure 2), a model with at least three states

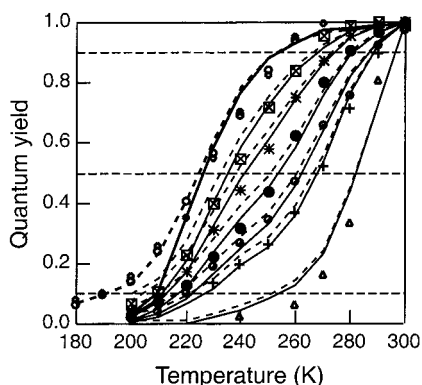


FIGURE 2: Temperature dependence of the quantum efficiency for the  $Q_A^-$  to  $Q_B$  electron transfer. At  $\Phi = 10\%$ ,  $50\%$ , and  $90\%$   $k_{(A)B} = 1, 10,$  and  $100 \text{ s}^{-1}$ , respectively. pH of the sample at room temperature:  $\diamond$ , pH 6.0;  $\circ$ , pH 8.0;  $\square$  (with  $\times$  within), pH 9.3;  $*$ , pH 9.6;  $\bullet$ , pH 9.8;  $\oplus$ , pH 10.0;  $+$ , pH 10.2;  $\triangle$ , pH 10.5. The solid line is the result of the simulation using model I (Figure 3) and the dashed line model II. The pH value is allowed to shift by no more than 0.1 pH unit from the measured value to improve the fit. The reaction free energies and barrier heights derived from the fit to model 1 are provided in Tables 1 and 2.

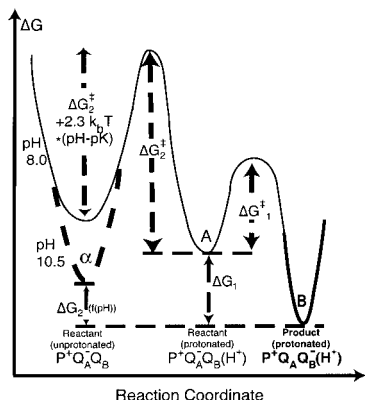


FIGURE 3: Reaction coordinate for electron transfer from  $Q_A^-$  to  $Q_B$ . Three states are shown:  $\alpha$ , the unprotonated, and A, the protonated reactant state ( $P^+Q_A^-$ ) and B, the protonated product ( $P^+Q_B^-$ ). The free energy difference and barrier between A and B are assumed to be pH independent. However, A and B shift with respect to  $\alpha$  as the pH changes.

is needed (Figure 3). The reactant  $P^+Q_A^-$  redox state can be protonated (A) or unprotonated ( $\alpha$ ). The two populations are in equilibrium with an apparent  $pK_\alpha$  of 9.7 (room temperature values of the pH are given). The product state (B) is assumed to be always protonated. Below pH 8 there is less than 0.3 proton bound from solution on electron transfer from  $Q_A^-$  to  $Q_B$  (45, 46). Thus, protonated reactant and product states have essentially the same number of protons bound, so as the pH changes, the energy of A and B changes by the same amount, keeping  $\Delta G_{AB}$  constant. A and B may shift relative to the ground state, but this will not influence the reactions considered here. However, the A and B states shift relative to  $\alpha$ . Thus,  $\Delta G_{AB}$  is assumed to be pH independent, while the free energy of the reaction from the unprotonated reactant ( $\Delta G_{\alpha B}$ ) is pH dependent with

$$\Delta G_{\alpha B} = \Delta G_{AB} + 2.3k_bT(\text{pH} - pK_\alpha) \quad (2)$$

$T$  is the temperature, and  $k_b$  is the Boltzman constant. The rate-determining step for electron transfer depends on the pH. At low pH the reactant is in the A state and the barrier

is  $\Delta G_{AB}^+$ . At high pH RCs are in the unprotonated ( $\alpha$ ) reactant state. Now the taller, pH-dependent proton uptake barrier must be crossed.  $\Delta G_{A\alpha}^+$  is the barrier for the pH-independent transformation from A to  $\alpha$ . The forward direction activation energy for proton binding ( $\Delta G_{\alpha A}^+$ ) is  $\Delta G_{A\alpha}^+ + 2.3k_bT(\text{pH} - pK_\alpha)$ . When the pH is near  $pK_\alpha$ , there is initially a mixed population of protonated and unprotonated reactant. Both are seen in the stretched temperature dependence of  $\Phi$  because at low temperature  $k_{\alpha A}$  is enough slower than  $k_{AB}$  that  $\alpha$  and A do not remain at equilibrium during the lifetime of the  $P^+Q_A^-$  state. If  $\Delta G_{AB}$  and  $\Delta G_{\alpha B}$  are known, then the dependence of  $\Phi$  on temperature will provide  $\Delta G_{AB}^+$  and  $\Delta G_{\alpha B}^+$  and the associated activation entropies and enthalpies.

*Free Energy, Enthalpy, and Entropy Change between A,  $\alpha$ , and B.* In RCs the equilibrium constant between  $P^+Q_A^-$  and  $P^+Q_B^-$  can be determined in situ from the rate at which  $P^+Q_B^-$  returns to the ground state ( $PQ_AQ_B$ ) ( $k_{BP}^{\text{obs}}$ ) (44, 47, 48). There are two pathways for charge recombination. One is direct electron tunneling from  $Q_B^-$  to  $P^+$  (at  $k_{BP}$ ). The second is an uphill pathway re-forming  $P^+Q_A^-$ , which then returns to the ground state. At room temperature, the indirect pathway is dominant, while as the temperature falls, this slows so now the direct route is used. The rate of the indirect process is dependent on the fraction of RCs in the  $P^+Q_A^-$  (A or  $\alpha$ ) state and so monitors the equilibrium constant between B and the reactant substates. At physiological pH, charge recombination goes from the protonated product (B) through the protonated reactant (A) back to the ground state (Figure 3). The pH-independent free energy difference is  $\Delta G_{AB}$ . At high pH the protonated product equilibrates with the unprotonated reactant ( $\alpha$ ) with  $\Delta G_{B\alpha}^+ = \Delta G_{AB} + 2.3k_bT(\text{pH} - pK_\alpha)$ . At room temperature,  $\Delta G_{AB} = \Delta G_{\alpha B}$  at pH 9.7, identifying this as the  $pK_\alpha$  for proton uptake. Assuming equilibrium between A,  $\alpha$ , and B, the charge recombination rate is

$$k_{BP}^{\text{obs}} = k_{BP} + k_{AP}[A] + k_{\alpha P}[\alpha] = k_{BP} + \frac{k_{AP}e^{-\Delta G_{BA}/k_bT} + k_{\alpha P}e^{-\Delta G_{B\alpha}/k_bT}}{1 + e^{-\Delta G_{BA}/k_bT} + e^{-\Delta G_{B\alpha}/k_bT}} \quad (3a)$$

The  $P^+Q_A^-$  charge recombination rate ( $k_{AP}$ ) is relatively pH independent so  $k_{\alpha P}$  is assumed to equal  $k_{AP}$ . Equation 2 can then be transformed to recover the more familiar formula (44, 47, 48):

$$k_{BP}^{\text{obs}} = k_{BP} + \frac{k_{AP}}{1 + 1/(e^{-\Delta G_{BA}/k_bT} + e^{-\Delta G_{B\alpha}/k_bT})} = k_{BP} + \frac{k_{AP}}{1 + K_{AB}} \quad (3b)$$

where  $K_{(A)B}$  is the measured equilibrium constant between  $P^+Q_B^-$  (B) and  $P^+Q_A^-$  (A and/or  $\alpha$ ) found at a given pH and temperature. Both  $k_{(A)P}$  (42, 43) and  $k_{BP}$  (17, 49) are only slightly temperature dependent above 200 K.  $k_{(A)P}$  is assigned to be  $10 \text{ s}^{-1}$  and  $k_{BP}$   $0.1 \text{ s}^{-1}$  (17, 50–52). The temperature dependence of  $\Delta G_{AB}$  is determined at pH 8.0 where  $P^+Q_A^-$  is fully protonated, while the temperature dependence of  $\Delta G_{\alpha B}$  is determined at pH 10.5 where the unprotonated  $\alpha$  state predominates (Table 1).

Table 1: Reaction Thermodynamics for the  $\alpha$ , A, and B Substates<sup>a</sup>

meV at 298 <sup>c</sup>	$\alpha$ to B (pH 10.5) $\Delta G_{\alpha\beta}$	=	A to B (pH 8.0) <sup>b</sup> $\Delta G_{AB}^{\circ}$	+	RC proton uptake (pH 10.5) <sup>d</sup> $2.3k_bT(\text{pH}_{25^{\circ}\text{C}} - \text{p}K_{\alpha})$	+	temp correction buffer pH (pH <sub>T</sub> ) <sup>e</sup> $2.3k_bT(\text{pH}_T - \text{pH}_{24^{\circ}\text{C}})$
$\Delta G$	$-45 \pm 5$	=	$-90 \pm 10$	+	$45 \pm 11$	+	0
$\Delta H$	$-330 \pm 10$	=	$-230 \pm 20$	+	$-603 \pm 22$	+	$503 \pm 1$
$-\Delta S$	$-(-285 \pm 10)$	=	$-(-140 \pm 20)$	+	$-(-648 \pm 22)$	+	$-(503 \pm 1)$

<sup>a</sup> The equilibrium free energy, enthalpy, and entropy change between A,  $\alpha$ , and B are derived from Figure 4. <sup>b</sup>  $\Delta G_{AB}$  is measured at pH 8 and is assumed to be pH independent. <sup>c</sup>  $\Delta S$  and the resultant  $\Delta G$  are given at 298 K.  $\Delta H$  is assumed to be temperature independent. <sup>d</sup> Assuming the Caps buffer pH (10.5 at 298 K) is temperature independent. The parameters for proton uptake by RCs are derived from the data in the other three columns. <sup>e</sup> Correction for the buffer pK shift.  $\text{pH}_T$  is the pH at the temperature of measurement calculated given the buffer proton dissociation enthalpy (39). The room temperature Caps pK is 10.4.

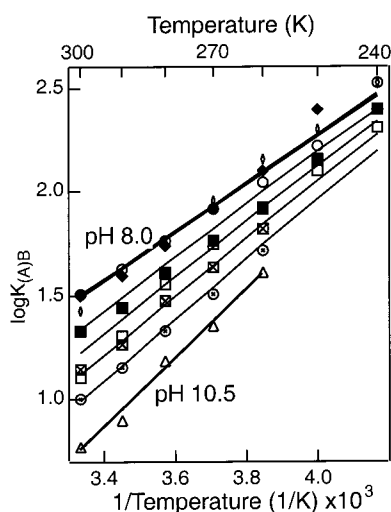


FIGURE 4: Temperature dependence of the equilibrium constant  $K_{(A)B}$  between  $\text{P}^+\text{Q}_A^-$  (A and  $\alpha$  substates) and  $\text{P}^+\text{Q}_B^-$  calculated from the rate of charge recombination (eq 3). The temperature dependence of  $K_{AB}$  is determined from the data at pH 8.0 and for  $K_{\alpha A}$  at pH 10.5. At intermediate pHs the equilibrium constant is obtained, given  $\Delta G_{\alpha B} = \Delta G_{\alpha B}(\text{at pH 10.5}) + 2.3k_bT(\text{pH} - 10.5)$  which assumes that the difference in pH of the different buffers is temperature independent. The parameters obtained are given in Table 2. Symbols:  $\blacklozenge$ , pH 7.0;  $\blacksquare$ , pH 8.7;  $\square$ , pH 9.0. The symbols at other pHs are the same as in Figure 2.

At an arbitrary pH  $\Delta G_{\alpha B}$  is assumed to be  $\Delta G_{\alpha B}(\text{at pH 10.5}) + 2.3k_bT(\text{pH} - 10.5)$ . The room temperature pH is used here. The solution pH is quite temperature dependent. However, the buffers used (Tris, Ches, and Caps) have very similar temperature dependence (36–39). The estimate of  $\Delta G_{\alpha B}$  thus assumes that the pH differs from the buffer at pH 10.5 (298 K) by the same amount at all temperatures. The lines for  $K_{AB}$  at intermediate pHs in Figure 4 are thus not the best fit to  $k_{BP}^{\text{obs}}$  but are derived from  $\Delta G_{AB}$  determined at the lowest pH,  $\Delta G_{\alpha B}$  obtained at the highest pH, and the assumption that the difference in pH of different samples is the same at each temperature.

The equilibrium constant  $K_{AB}$  was determined down to 240 K at pH 8.0 while at pH 10.5 it was only measured to 260 K because  $\Phi$  falls to zero at this pH and temperature (Figure 4). The back-reaction rate,  $k_{BP}^{\text{obs}}$ , is 2-fold slower in 60% glycerol than in aqueous solution even at room temperature and low pH. Thus,  $\Delta G_{AB}$  is 20 meV more favorable in this cryosolvent. This change has been previously ascribed to dehydration of the protein due to the osmotic stress from the glycerol used in the cryosolvent (41).

The reaction entropy and enthalpy are derived from the temperature dependence of the equilibrium constant (Table

1). Again the temperature dependence at pH 8.0 is used to determine the thermodynamic parameters for the electron transfer between protonated reactant and product, while measurements at pH 10.5 provide the entropy and enthalpy for the reaction from state  $\alpha$  to state B.  $\Delta G_{\alpha B}$  depends on the temperature dependence of the pH, which is a function of the buffer  $\Delta H$ . The buffer  $\Delta S$  and  $\Delta H$  were obtained from the literature (39).

The thermodynamics of the reactions connecting  $\alpha$  and A with B are given in Table 1. At pH 10.5 the entropy of the three states is ordered  $B < A < \alpha$  ( $\alpha$  the most favorable), while the enthalpy is also ordered  $B < A < \alpha$  (B the most favorable). Thus, electron transfer to  $\text{Q}_B$  from either  $\text{P}^+\text{Q}_A^-$  substate has a modest, favorable driving force with a favorable  $\Delta H$  and unfavorable  $\Delta S$ . Each reaction becomes more favorable with decreasing temperature. Since the  $\alpha$  to B reaction has a larger  $\Delta S$ ,  $\Delta G_{\alpha B}$  is somewhat more temperature dependent than  $\Delta G_{AB}$ . Thus,  $\text{p}K_{\alpha}$  shifts to higher pH as the temperature is decreased, so  $\text{p}K_{\alpha}$  changes from 9.7 (298 K) to  $\approx 13.5$  (200 K). The buffer pK also decreases with increasing temperature, so a Caps solution at pH 10.5 (298 K) would shift to have a pH of  $\approx 13.5$  at 200 K.

The  $\alpha$  to B reaction is a two-step process. One is the transition from A to B which was investigated directly at low pH. The other is the transition from  $\alpha$  to A which is subdivided here into the proton binding by the RCs if the pH were assumed to be temperature independent and a second term which provides a correction for the change in pH with temperature. At pH 10.5, above  $\text{p}K_{\alpha}$  at 298 K, proton binding is unfavorable. Proton binding to RCs has a favorable enthalpy and unfavorable entropy. The temperature correction to the pH, accounting for the energetics of buffer deprotonation, adds an unfavorable enthalpy and favorable entropy term to  $\Delta G_{\alpha B}$ . The solution pH increases with temperature, at a rate that is somewhat smaller than the change in RC  $\text{p}K_{\alpha}$ .

*Kinetic Simulation of the Barriers for Electron Transfer.* The rate of formation of B at a given pH and temperature is determined from the quantum efficiency ( $\Phi$ ) using eq 1 (Figure 3). The theoretical lines through the data represent a simulation given the following kinetic model.

(1) The reaction rate can be obtained assuming that state A can go on to  $\alpha$  (at  $k_{A\alpha}$ ) to B (at  $k_{AB}$ ) or to the ground state (at  $k_{AP}$ ) and is formed from  $\alpha$  (at  $k_{\alpha A}$ ) or B ( $k_{BA}$ ). State  $\alpha$  can go to A or the ground state and is re-formed from A. State B can go to A or the ground state and is formed from A. State B and  $\alpha$  do not interconvert directly but must pass through A. Formation of the ground state is irreversible. Thus, there are six rate constants ( $k_{AB}$  and  $k_{BA}$ ;  $k_{A\alpha}$  and  $k_{\alpha A}$ ;

Table 2: Barriers Separating the  $\alpha$ , A, and B Substates<sup>a</sup>

meV	$\Delta G^\ddagger$ (298 K)	=	$\Delta H^\ddagger$	–	$T\Delta S^\ddagger$ (298 K)
$\Delta G_{AB}^\ddagger$	$500 \pm 100$	=	$420 \pm 80$	–	$-80 \pm 60$
$\Delta G_{A\alpha}^\ddagger$	$620 \pm 60$	=	$830 \pm 50$	–	$210 \pm 40$

<sup>a</sup> Parameters are the outcome of a kinetic simulation using model I and the reaction thermodynamic parameters in Table 1. The results of this model are compared with the experiment in Figure 2.

$k_{AP}$  and  $k_{BP}$ ). All reactions which do not involve  $\alpha$  are unimolecular, with rates that depend only on the reactant concentration and a unimolecular rate constant. As before,  $k_{AP}$  is taken as  $10 \text{ s}^{-1}$  and  $k_{BP}$  as  $0.1 \text{ s}^{-1}$ .

(2) The rate of electron transfer between A and B is

$$k_{AB} = \frac{k_b T}{h} \exp\left[\frac{\Delta S_{AB}^\ddagger}{k_b}\right] \exp\left[-\frac{\Delta H_{AB}^\ddagger}{k_b T}\right]$$

$$k_{BA} = k_{AB} \exp\left[\frac{\Delta S_{BA}}{k_b}\right] \exp\left[-\frac{\Delta H_{BA}}{k_b T}\right] \quad (4)$$

$h$  is Planck's constant.

(3) The electron transfer from  $\alpha$  to A is bimolecular as it depends on proton binding. The pseudo-first-order rate  $k_{\alpha A}$  is

$$k_{\alpha A} = k_0[\text{H}^+] = k_{A\alpha} \exp\left[\frac{\Delta S_{AB} - \Delta S_{\alpha B}^{10.5}}{k_b}\right] \times$$

$$\exp\left[-\frac{\Delta H_{AB} - \Delta H_{\alpha B}^{10.5}}{k_b T}\right] \times 10^{\text{pH}-10.5} \quad (5)$$

where  $k_0$  is the pH-independent, second-order rate constant. The thermodynamic parameters for the reaction from A to B are pH independent. The values derived at pH 10.5 are used for the  $\alpha$  to B reaction. The  $10^{\text{pH}-10.5}$  term corrects the free energy to account for the change in proton concentration at the pH of measurement. The entropy and enthalpy at pH 10.5 are found in Table 1.

(4) The initial conditions assume that A and  $\alpha$  are at equilibrium given the pH and  $\text{p}K_\alpha$ , while there is no B. So

$$A(t=0) = \frac{1}{1 + 10^{\text{pH}-\text{p}K_\alpha}}$$

$$\alpha(t=0) = \frac{10^{\text{pH}-\text{p}K_\alpha}}{1 + 10^{\text{pH}-\text{p}K_\alpha}} \quad (6)$$

Given the kinetic model and the thermodynamic parameters in Table 1, the fraction of  $\text{P}^+\text{Q}_A^-$  that reaches the  $\text{P}^+\text{Q}_B^-$  state,  $\Phi$ , can be modeled as a function of pH. The activation energies, enthalpies, and entropies are given in Table 2. The simulation using the three-state model is generally consistent with the experimental data. Accurate assessment of the error for these parameters is difficult to obtain. However, limits were estimated from visual inspection to determine when the calculated  $\Phi$  no longer models the data.

The activation barriers are given relative to the protonated  $\text{P}^+\text{Q}_A^-$  state (A) (Figure 3). These are pH independent. The pH dependence of the reaction can be derived as described in eq 5. The second-order rate constant for proton uptake  $k_0$  is  $\approx 10^{12} \text{ M}^{-1} \text{ s}^{-1}$  (298 K). A smaller, perhaps more realistic,

bimolecular rate is obtained if the protonated buffer (buffer $\cdot\text{H}^+$ ) is the donor. Here the observed rate would be

$$k_0^{\text{obs}} = k_0[\text{buffer}\cdot\text{H}^+] \times 10^{(\text{p}K_{\text{acceptor}} - \text{p}K_{\text{donor}})} \quad (7)$$

With 10 mM buffer, a  $\text{p}K_{\text{acceptor}}$  of  $\approx 7$  (e.g., surface His), and  $\text{p}K_{\text{donor}} \approx 10$  for the buffer,  $k_0$  will be of the order of  $10^7$  when  $k_0^{\text{obs}}$  is  $\approx 10^2$  ( $\Phi \approx 50\%$ ). The nature of the proton donor and  $k_0$  rate do not affect the values in Tables 1 and 2.

The substantial  $\Delta H_{A\alpha}^\ddagger$  of 830 meV for A to release a proton (A to  $\alpha$ ) is twice that found for the barrier for electron transfer (A to B).  $\Delta S_{A\alpha}^\ddagger$  is actually favorable ( $-210 \text{ meV}$  at 298 K) while  $\Delta S_{AB}^\ddagger$  is moderately unfavorable. In each case the ranking of the barriers is consistent with the relative free energy change of the respective reactions. Thus, moving from A to B has a favorable  $\Delta H$ , while A to  $\alpha$  does not. In contrast,  $\alpha$  has a larger entropy than A.

*Model II.* The simulation predicts that the quantum yield at low pH will decay faster at low temperature than is found (Figure 2). This suggests the presence of a protonated reactant state with a smaller barrier to reaction. A state of this kind has been previously characterized (17, 23). Model I was therefore modified to include an active state ( $A^*$ ) in equilibrium with the other two  $\text{P}^+\text{Q}_A^-$  states (A and  $\alpha$ ). The barrier to the  $\text{Q}_A^-$  to  $\text{Q}_B^-$  electron transfer in this conformation is assumed to be so low that the electron transfer from  $A^*$  does not slow significantly with temperature. Thus,  $A^*$  is  $\approx 40 \text{ meV}$  above the protonated  $\text{P}^+\text{Q}_A^-$  state and proceeds to  $\text{P}^+\text{Q}_B^-$  instantaneously after the actinic flash. For simplicity  $\Delta S_{AA^*}$  is assumed to be zero. The equations for model I remain the same, and only the initial condition is changed to

$$A(t=0) = \frac{1}{1 + 10^{\text{pH}-\text{p}K_\alpha} + e^{-\Delta G_0/k_b T}}$$

$$\alpha(t=0) = \frac{10^{\text{pH}-\text{p}K_\alpha}}{1 + 10^{\text{pH}-\text{p}K_\alpha} + e^{-\Delta G_0/k_b T}} \quad (8)$$

$$B(t=0) = A^*(t=0) = \frac{e^{-\Delta G_0/k_b T}}{1 + 10^{\text{pH}-\text{p}K_\alpha} + e^{-\Delta G_0/k_b T}}$$

The results of the two simulations are compared in Figure 2. The low-temperature tail of the freeze out curve at low pH is fitted better with model II. However, the quantum efficiency is overestimated in the pH region near  $\text{p}K_\alpha$ . Making  $\Delta G_{AB}^\ddagger$  smaller reduces this error, but now the quantum yield at low pH and low temperature is again underestimated. Thus, there are some systematic differences between the model and the data. Possible flawed assumptions are that only the level of  $\alpha$  shifts relative to other states when the pH is changed and that  $\Delta H$  and  $\Delta H^\ddagger$  are temperature independent. However, the current data set is not large enough to justify adding more parameters.

## DISCUSSION

The work presented here explores experimentally the reaction pathway for electron transfer from  $\text{Q}_A^-$  to  $\text{Q}_B^-$ . The reaction is not limited by the electron tunneling reaction itself but is gated by unknown conformational changes. This has been established by the observation that the reaction rate is independent of the reaction driving force (19, 22). In contrast,

RC reactions where electron tunneling is rate determining show the dependence on the driving force predicted by Marcus electron transfer theory (22, 40). The measurement of the rate as a function of temperature and pH allows a variety of reactant substates to be seen and the thermodynamic and kinetic parameters connecting these states to be determined.

The pH dependence of the  $Q_A^-$  to  $Q_B$  electron transfer has been previously measured at room temperature (53). The rate is constant below pH 9 and decreases with an apparent  $pK$  of 9.5. The model proposed here is fully consistent with this. It is well established that  $Q_B$  is not directly protonated in the semiquinone state (54), so the observed  $pK_a$  results from proton binding by amino acids close to  $Q_B$ . The kinetic measurements reported here cannot directly identify the atomic changes in the RCs that differentiate the A,  $\alpha$ , and  $A^*$  substates. However, several mutants have been found to have a pH dependence that is different from wild-type RCs at room temperature. For example, mutation of Glu L212, 4 Å from  $Q_B$ , to Gln eliminates the fall off in rate at high pH (55), while in the Asp L213 to Asn mutant the  $pK$  is shifted to below 7 (50). Glu L212 and/or the closely coupled Asp L213 are likely to be the proton binding site with a  $pK$  of  $\approx 9.5$  (30, 50, 55–58). The temperature dependence of  $\Phi$  is currently being investigated for several  $Q_B$  site mutants.

Three substates of  $P^+Q_A^-$  are used to simulate the temperature dependence of the rate of electron transfer. A single reactant state with a pH-dependent reaction barrier cannot yield the stretched, bimodal behavior of the freeze out curve at  $pH \sim pK_a$ . However, two substates (A and  $\alpha$ ) with a pH-dependent equilibrium between them can. Near  $pK_a$  at low temperature the rate of proton binding ( $k_{\alpha A}$ ) is slower than the rate of electron transfer in the protonated reactant ( $k_{AB}$ ) so both substates are seen in the reaction kinetics.

The model assumes a sequential mechanism where the unprotonated  $\alpha$  state must bind a proton to form A before B can be formed. Electron transfer in  $\alpha$  would lead to the formation of an unprotonated  $P^+Q_B^-$  state ( $\beta$ ) as an intermediate. The proton binding groups are predominately near  $Q_B$ . Thus, the energy difference between A and  $\alpha$  is modest as the electron on  $Q_A$  is interacting with ionized, acidic residues in the  $Q_B$  site (59, 60). In contrast, a  $\beta$  state would require  $Q_B^-$  to be formed quite close to a cluster of unprotonated acidic residues (30). Thus,  $\beta$  would be expected to be at much higher energy than B and so is ignored.

*Characterization of Active Substates at Low Temperature.* There is still a significant barrier between the A and B states. Given states  $\alpha$ , A, and B with the parameters in Tables 1 and 2, there should be no reaction below 200 K. However, the minimum quantum yield remains  $\approx 10\%$  at low pH (Figure 2). The free energy of  $P^+Q_A^-$  was previously found to rise by  $\approx 1$  meV/K below 210 K (16), decreasing the barrier between A and B favoring electron transfer. However, this correction to the simulation is too small to explain the observed residual activity. As described in model 2, equilibration of A with a nearby, active  $A^*$  substate  $\approx 40$  meV above A between flashes will yield the observed low-temperature activity.

When RCs are frozen in the light in the  $P^+Q_B^-$  state, the  $P^+Q_A^-$  subsequently formed on photoexcitation goes on to  $P^+Q_B^-$  with 100% quantum yield even at temperatures below 40 K (17, 23). Thus, light-adapted RCs return to the ground

state in a high-energy substate where the conformational changes required for reaction are frozen in. Preliminary measurements suggest that electron transfer occurs in less than 10  $\mu s$  at 40 K (Xu and Gunner, unpublished results). This rate is closer to that found in RCs where electron transfer is rate limiting (22) than to the 100  $\mu s$  rate found at room temperature for the gated reaction (19, 22).

When the temperature of light-adapted RCs is raised to  $\approx 200$  K, the active RCs establish an equilibrium with an inactive population on the minutes time scale. Thus, in both dark-adapted RCs as well as in light-adapted protein (17) at  $\approx 200$  K there an inactive state (A here) in equilibrium with an active form ( $A^*$ ). Approximately 10% of the RCs are in the  $A^*$  state (Figure 2), while  $\approx 30\%$  of the light-adapted RCs remain active at the same temperature. The active fraction is used to estimate that  $A^*$  is  $\approx 40$  meV above A while in the light-adapted RCs the active and inactive states are separated by a smaller amount ( $\approx 20$  meV).

The inactive substate found in light-adapted RCs appears to be higher in energy than the inactive dark-adapted state, A. Since active and inactive substates are in equilibrium, this implies that the active substates in light- and dark-adapted RCs are different. The light-adapted RCs may freeze in many changes that occur on formation of a relaxed B state at room temperature while  $A^*$  has only the minimum conformational changes needed for electron transfer. The  $P^+Q_B^-$  substates formed in light- and dark-adapted protein would then be different. Presumably in the dark-adapted RCs the product is more similar to the reactant and at higher energy. Thus, there are multiple inactive and active substates that can be characterized in properly prepared protein.

*Possible Sources of the Reaction  $\Delta S$ .* From A or  $\alpha$  to B the reaction has a favorable enthalpy and unfavorable entropy. The  $Q_A$  site is fairly rigid. From room temperature to  $\approx 200$  K reduction of  $Q_A$  by  $BPh^-$  has little  $\Delta S$  (16, 61). Thus the  $Q_B$  site is likely to be the source of the changes that underlie  $\Delta S_{AB}$  and  $\Delta S_{\alpha B}$ . It has been suggested that the cluster of acidic residues exists in a distribution of ionization states with different locations of polar side chains in the ground, A, or  $\alpha$  states (30, 58). In particular, Glu L212 or Asp L213 and L210 may share one or two protons so each is only partially ionized. In addition,  $Q_B$  itself may be distributed between the distal and proximal sites (12, 62) in an equilibrium that depends on the ionization state of the acidic cluster (32, 34). There are only modest differences between the energies of these different microstates (30). In contrast, in the B state the charge on  $Q_B^-$  reorganizes these groups. Now  $Q_B^-$  is only in the proximal binding site, and the nearby L212 and L213 are neutral. These changes stabilize the B state, so  $\Delta H$  is favorable but would reduce the entropy of the system.

*Temperature Dependence of the Solution pH.* There is little proton uptake moving between the A and B states (46) so this reaction is treated as being pH independent. However, a proton is bound in the transition between  $\alpha$  and A states. The temperature dependence of the buffer pH creates problems for any thermodynamic analysis of pH-dependent reactions. Remarkably, in RCs it is possible to determine reaction free energies in situ using rates of reactions which involve preequilibration with a higher energy state (eq 3, Figure 4). Thus,  $\Delta G_{AB}$  and  $\Delta G_{\alpha B}$  and their temperature dependence are determined here at the same time as the

electron transfer from  $Q_A^-$  to  $Q_B$  is measured (Table 1). However, the buffer temperature dependence does influence  $\Delta G_{\text{QB}}$ . This contribution must be removed to obtain the thermodynamic parameters connecting the protonated and unprotonated  $P^+Q_A^-$  states A and  $\alpha$ . The temperature dependence of various buffers has been measured previously in aqueous solution from 0 to 50 °C (36, 39) or in cryosolvent from -50 to 20 °C (37, 38). The temperature dependence of the buffers used here was reported to be about  $-0.03/^\circ\text{C}$ , except for Mes and Hepes where the value is  $-0.01/^\circ\text{C}$ . The change in pH measured here between 278 and 298 K in the glycerol/buffer mixture is consistent with earlier reports. Given the literature values for the Caps buffer  $\Delta H$ , the contribution of proton binding to RCs can be extracted from the measured thermodynamic parameters for the  $\alpha$  to A transition. Proton binding, presumably into the ionized acidic cluster near  $Q_B$ , has a favorable  $\Delta H_{\alpha A}$  and unfavorable  $\Delta S_{\alpha A}$ .

**Barriers between Substates.** The temperature dependence of the  $Q_A^-$  to  $Q_B$  electron transfer rate at neutral pH has been measured previously near room temperature (20, 21). These measurements follow spectral shifts associated with the reaction providing a lifetime of  $\approx 100 \mu\text{s}$  for the reaction at room temperature. Early studies where the kinetics were fit by one exponential provided an activation enthalpy of 14.3 kcal/mol (47). In more recent results, the electron transfer kinetics were resolved into two exponential phases, with  $\Delta H^\ddagger$  of 2.7–4.5 kcal/mol. A slower phase, which has been identified as monitoring primarily relaxation following the electron transfer, has an  $\Delta H^\ddagger$  of 9.5–11.5 kcal/mol (20, 21). The  $\Delta H_{\text{AB}}^\ddagger$  of 9.7 kcal/mol determined here is closer to the slowest room temperature transients. However, the use of  $\Phi$  to measure the rate is only sensitive when  $k_{\text{AB}}$  or  $k_{\alpha B}$  is near the competing  $k_{\text{AP}}$ . Thus, at each pH the rate can only be determined over a limited temperature range. While the simple model shown here simulates the entire data set fairly well, future measurements will be needed to directly measure the rate of  $Q_B$  reduction, better connecting low and room temperature results.

**Heterogeneous Reaction Kinetics.** One significant approximation in the model is that each substate is treated as a homogeneous population with single exponential rate constants connecting them. This assumption is used when  $k_{\text{(A)B}}$  is derived from  $\Phi$  (eq 1) and in the kinetic simulation. In the real protein each substate is likely to consist of an inhomogeneous population of individual microstates so reaction kinetics will show distributed rates (63, 64). The conversion among the microstates is usually fast enough at room temperature so the reaction appears homogeneous. However, direct measurements of electron transfer from  $Q_A^-$  to  $Q_B$  show increasingly inhomogeneous kinetics when the temperature is lowered (20). Thus, part of the measured rate falloff with temperature will not be due to the barriers between A,  $\alpha$ , and B as assumed here. Rather, the increasing importance of slower individual microstates within each substate also plays a role. This increases the temperature dependence, causing both  $\Delta H^\ddagger$  and the rate extrapolated to infinite temperature to be too large. For example, if the rate were distributed over 2 orders of magnitude at 200 K,  $\Delta H^\ddagger$  would be 30% smaller, decreasing the height of the estimated barrier, while  $\Delta S^\ddagger$  would be  $\approx 120 \text{ meV}$  (298 K) less favorable than reported here.

**Bimolecular Rate Constant for Proton Binding.** Previous measurements of the temperature dependence of the Caps buffer pK (39) allows independent consideration of the RC and buffer contribution to the thermodynamics of the A and  $\alpha$  reaction. However, proton release by the buffer, proton binding by the RCs, internal proton transfer, or other motions in the protein are all candidates for the rate-determining step whose barrier is being measured. The apparent bimolecular rate constant of  $10^{12} \text{ M}^{-1} \text{ s}^{-1}$  for the proton uptake (298 K) is larger than expected for a simple diffusion-limited reaction (65). However, this is consistent with earlier measurements in RCs. The bimolecular rate of proton binding to  $P^+Q_A^-$  RCs was found to be  $2 \times 10^{13} \text{ M}^{-1} \text{ s}^{-1}$  at pH 10 at room temperature (66). The rate was weakly viscosity dependent and had a larger activation energy ( $>350 \text{ meV}$ ) than expected for diffusion of a proton (80–150 meV) (66). The rate-determining step for proton binding was proposed to be internal proton motions rather than proton diffusion itself. The bimolecular rate constant determined here is smaller than in the previous room temperature measurements while the activation energy is larger. The overestimate of  $\Delta H_{\text{QB}}^\ddagger$  due to the assumption of a homogeneous reaction rate may contribute. In addition, the reaction is being determined at a much lower temperature here, and the discrepancy could be due to temperature dependence of  $\Delta H_{\text{QB}}^\ddagger$ . Last, the earlier values monitor proton uptake directly while the measurements here follow the rate of formation of a state which is competent to support electron transfer to  $Q_B$ . Thus, there may be additional barriers in the formation of the A substate that are missed when proton uptake is measured directly.

## CONCLUSION

High-resolution structural studies of proteins can show what atoms move when a reaction occurs. It can even be possible to obtain structures for discrete trapped reaction intermediates. However, the structures themselves do not show the energy of the different substates or the activation barriers between them. Rather, these can be determined from the analysis of the temperature dependence of rates and substate equilibrium constants. The challenge is then to make the connection between the atomic structure and the substate energy landscape. Detailed kinetic and thermodynamic measurements where the protein, substrate, or external conditions such as pH are changed can begin to identify the structural features that underlie the rate-determining events.

## ACKNOWLEDGMENT

The authors thank Drs. Colin Wraight and Melvin Okamura for stimulating discussions and Mark Paddock for the suggestion that protonated buffer can be the kinetically competent proton donor.

## REFERENCES

1. Frauenfelder, H., Sligar, S. G., and Wolynes, P. G. (1991) *Science* 254, 1598–1603.
2. Zaccari, G. (2000) *Science* 288, 1604–1607.
3. Parak, F., Knapp, E. W., and Kucheida, D. (1982) *J. Mol. Biol.* 161, 177–194.
4. Doster, W., Cusack, S., and Petry, W. (1989) *Nature* 337, 754–756.
5. Loncharich, R. J., and Brooks, B. R. (1990) *J. Mol. Biol.* 215, 439–455.

6. Vitcup, D., Ringe, D., Petsko, G. A., and Karplus, M. (2000) *Nat. Struct. Biol.* 7, 34–38.
7. Genick, U. K., Borgstahl, G. E. O., Ng, K., Ren, Z., Pradervand, C., Burke, P. M., Srajer, V., Teng, T., Schildkamp, W., McRee, D. E., Moffat, K., and Getzoff, E. D. (1997) *Science* 275, 1471–1475.
8. Srajer, V., Teng, T., Ursby, T., Pradervand, C., Ren, Z., Adachi, S., Schildkamp, W., Bourgeois, D., Wulff, M., and Moffat, K. (1996) *Science* 274, 1726–1729.
9. Luecke, H., Schobert, B., Richter, H. T., Cartailler, J. P., and Lanyi, J. K. (1999) *Science* 286, 255–261.
10. Petsko, G. A., and Ringe, D. (2000) *Curr. Opin. Chem. Biol.* 4, 89–94.
11. Schlichting, I., and Chu, K. (2000) *Curr. Opin. Struct. Biol.* 10, 744–752.
12. Stowell, M. H. B., McPhillips, T. M., Rees, D. C., Soltis, S. M., Abresch, E., and Feher, G. (1997) *Science* 276, 812–816.
13. Deng, H., Zhadin, N., and Callender, R. (2001) *Biochemistry* 40, 3767–3773.
14. Lee, A. L., and Wand, A. J. (2001) *Nature* 411, 501–504.
15. Volkman, B. F., Lipson, D., Wemmer, D. E., and Kern, D. (2001) *Science* 291, 2429–2433.
16. Xu, Q., and Gunner, M. R. (2000) *J. Phys. Chem. B* 104, 8035–8043.
17. Xu, Q., and Gunner, M. R. (2001) *Biochemistry* 40, 3232–3241.
18. Blankenship, R. E., Madigan, M. T., and Bauer, C. E. (1995) *Anoxygenic Photosynthetic Bacteria*, Vol. 2, Kluwer Academic Publishers, Amsterdam.
19. Graige, M. S., Feher, G., and Okamura, M. Y. (1998) *Proc. Natl. Acad. Sci. U.S.A.* 95, 11679–11684.
20. Tiede, D. M., Vazquez, J., Cordova, J., and Marone, A. P. (1996) *Biochemistry* 35, 10763–10775.
21. Li, J., Gilroy, D., Tiede, D. M., and Gunner, M. R. (1998) *Biochemistry* 37, 2818–2829.
22. Li, J., Takahashi, E., and Gunner, M. R. (2000) *Biochemistry* 39, 7445–7454.
23. Kleinfeld, D., Okamura, M. Y., and Feher, G. (1984) *Biochemistry* 23, 5780–5786.
24. Lancaster, R., and Michel, H. (1997) *Structure* 5, 1339–1359.
25. Nabedryk, E., Bagley, K. A., and Thibodeau, D. L. (1990) *FEBS Lett.* 266, 59–62.
26. Brzezinski, P., and Andreasson, L. E. (1995) *Biochemistry* 34, 7498–7506.
27. Cherepanov, D. A., Bibikov, S. I., Bibikova, M. V., Bloch, D. A., Drachev, L. A., Gupta, O. A., Osterheld, D., Semenov, A. Y., and Mulikidjanian, A. Y. (2000) *Biochim. Biophys. Acta* 1459, 10–34.
28. van Mourik, F., Reus, M., and Holzwarth, A. R. (2001) *Biochim. Biophys. Acta* 1504, 311–318.
29. Lancaster, C. R. D., Michel, H., Honig, B., and Gunner, M. R. (1996) *Biophys. J.* 70, 2469–2492.
30. Alexov, E., and Gunner, M. (1999) *Biochemistry* 38, 8253–8270.
31. Sham, Y. Y., Muegge, I., and Warshel, A. (1999) *Proteins* 36, 484–500.
32. Grafton, A. K., and Wheeler, R. A. (1999) *J. Phys. Chem. B* 103, 5380–5387.
33. Rabenstein, B., Ullmann, G. M., and Knapp, E. W. (2000) *Biochemistry* 39, 10487–10496.
34. Zachariae, U., and Lancaster, C. R. (2001) *Biochim. Biophys. Acta* 1505, 280–290.
35. Goldsmith, J. O., and Boxer, S. G. (1996) *Biochim. Biophys. Acta* 1276, 171–175.
36. Good, N. E., Winget, G. D., Winter, W., Connolly, T. N., Izawa, S., and Singh, R. M. (1966) *Biochemistry* 5, 467–477.
37. Maurel, P., Hoa, G. H., and Douzou, P. (1975) *J. Biol. Chem.* 250, 1376–1382.
38. Taylor, M. J., and Pignat, Y. (1982) *Cryobiology* 19, 99–109.
39. Fukada, H., and Takahashi, K. (1998) *Proteins* 33, 159–166.
40. Gunner, M. R., and Dutton, P. L. (1989) *J. Am. Chem. Soc.* 111, 3400–3412.
41. Tiede, D. M., Utschig, L., Hanson, D. K., and Gallo, D. M. (1998) *Photosynth. Res.* 55, 267–273.
42. McElroy, J. D., Mauzerall, D. C., and Feher, G. (1974) *Biochim. Biophys. Acta* 333, 261–277.
43. Gunner, M. R., Robertson, D. E., and Dutton, P. L. (1986) *J. Phys. Chem.* 90, 3783–3795.
44. Kleinfeld, D., Okamura, M. Y., and Feher, G. (1984) *Biochim. Biophys. Acta* 766, 126–140.
45. Maroti, P., and Wraight, C. A. (1988) *Biochim. Biophys. Acta* 934, 329–347.
46. McPherson, P. H., Okamura, M. Y., and Feher, G. (1988) *Biochim. Biophys. Acta* 934, 348–368.
47. Mancino, L. J., Dean, D. P., and Blankenship, R. E. (1984) *Biochim. Biophys. Acta* 764, 46–54.
48. Wraight, C. A., and Stein, R. R. (1980) *FEBS Lett.* 113, 73–77.
49. Hoff, A. J., de Boer, A. L., de Wijn, R., Neerken, S., Borovykh, I. V., Permentier, H. P., Paschenko, S. V., Vijgenboom, E., and Gast, P. (2001) *Biophys. J.* 80 (Part 2), 119.
50. Takahashi, E., and Wraight, C. A. (1992) *Biochemistry* 31, 855–866.
51. Labahn, A., Paddock, M. L., McPherson, P. H., Okamura, M. Y., and Feher, G. (1994) *J. Phys. Chem.* 98, 3417–3423.
52. Labahn, A., Bruce, J. M., Okamura, M. Y., and Feher, G. (1995) *Chem. Phys.* 97, 355–366.
53. Kleinfeld, D., Okamura, M. Y., and Feher, G. (1985) *Biochim. Biophys. Acta* 809, 291–310.
54. Lavergne, J., Matthews, C., and Ginet, N. (1999) *Biochemistry* 38, 4542–4552.
55. Paddock, M. L., Rongey, S. H., Feher, G., and Okamura, M. Y. (1989) *Proc. Natl. Acad. Sci. U.S.A.* 86, 6602–6606.
56. Hienerwadel, R., Grzybek, S., Fogel, C., Kreutz, W., Okamura, M. Y., Paddock, M. L., and Breton, J. (1995) *Biochemistry* 34, 2832–2843.
57. Breton, J., and Nabedryk, E. (1998) *Photosynth. Res.* 55, 301–307.
58. Rabenstein, B., Ullmann, G. M., and Knapp, E.-W. (1998) *Biochemistry* 37, 2488–2495.
59. Kalman, L., and Maroti, P. (1994) *Biochemistry* 33, 9237–9244.
60. Alexov, E., Miksovskaja, J., Baciou, L., Schifer, M., Hanson, D., Sebban, P., and Gunner, M. R. (2000) *Biochemistry* 39, 5940–5952.
61. Woodbury, N. W., Parson, W. W., Gunner, M. R., Prince, R. C., and Dutton, P. L. (1986) *Biochim. Biophys. Acta* 851, 6–22.
62. Lancaster, C. R. D. (1998) *Biochim. Biophys. Acta* 1365, 143–150.
63. Austin, R. H., Beeson, K. W., Eisenstein, D. L., Frauenfelder, E. H., and Gunsalus, I. C. (1975) *Biochemistry* 24, 5355–5373.
64. McMahon, B. H., Muller, J. D., Wraight, C. A., and Nienhaus, G. U. (1998) *Biophys. J.* 74, 2567–2587.
65. Gutman, M., and Nachleil, E. (1990) *Biochim. Biophys. Acta* 1015, 391–414.
66. Maroti, P., and Wraight, C. A. (1997) *Biophys. J.* 73, 367–381.